Supplement to: Global sonde datasets do not support a mesoscale transition in the turbulent energy cascade

Thomas D. DeWitt

S1 A generalized anisotropic structure function

The two-dimensional structure function represented by Eqn. 9 in the main text is not the unique choice if we simply require Eqns. 7 to be recovered when $\Delta x = 0$ or $\Delta z = 0$. To obtain Eqn. 9, we added the requirement that isotropic turbulence is recovered when $H_h = H_v$ and $\varphi_v = \varphi_h$. Here we drop this assumption by adding an additional parameter η such that

$$\langle \Delta v(\Delta x, \Delta z)^2 \rangle = \left(\varphi_h^{\eta/H_h} \Delta x^{2\eta} + \varphi_v^{\eta/H_h} \Delta z^{H_v \eta / H_h} \right)^{H_h/\eta}. \tag{S1}$$

When $\eta = 1$, Eqn. 9 in the main text is recovered. Otherwise, Eqns. 7 are still obtained when $\Delta x = 0$ or $\Delta z = 0$, but isotropic turbulence cannot be recovered. Visually, the parameter η makes the isolines of Δv more or less "boxy," as shown in Fig. S1.

Fitting Eqn. S1, rather than Eqn. 9, to the empirical structure function (Fig. S2) resulted in best-fit values of $\phi_h = 0.015 \pm 0.007, \phi_v = 0.006 \pm 0.001, H_h = 0.34 \pm 0.02, H_v = 0.65 \pm 0.01$, and $\eta = 0.81 \pm 0.07$, which are close to the values reported in the main text for $\eta = 1$. The contour lines of the fit in Fig. S2 also provide a slightly better match to the empirical contour lines as compared to Fig. 7.

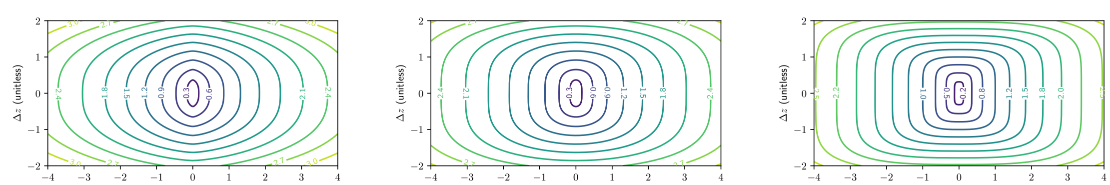

Figure S1: Countour plot of dimensionless form of Eqn. S1, as in Fig. 2 but for $\eta = 0.75$, $\eta = 1$, and $\eta = 1.5$. The value $\eta = 1$ was used in the main text.

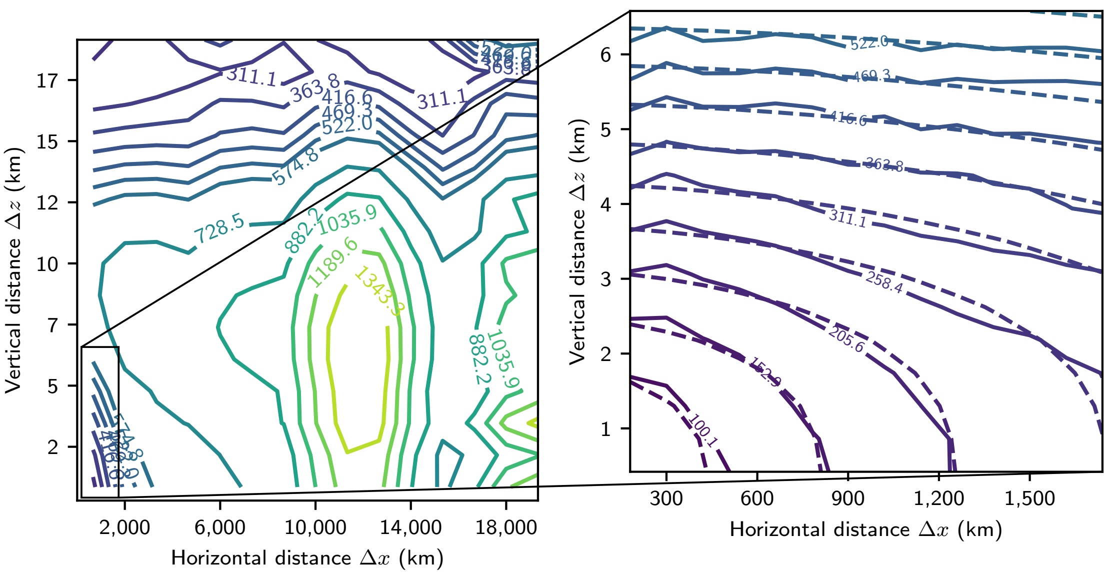

Figure S2: As in Fig. 7, but using Eqn. S1 for the fit.

S2 First and third order structure functions

In the main text we prefer second-order structure functions of velocity increments, which represent kinetic energy Δv^2, because they are most commonly examined in prior studies of turbulence. However, structure functions may be defined for arbitrary orders q as

$$\langle \Delta v^q \rangle \sim \Delta r^{\zeta(q)}. \tag{S2}$$

For a nonintermittent turbulent cascade, the structure function exponent $\zeta(q)$ is simply equal to qH. For the more realistic intermittent case, in general $\zeta(q) < qH$ for $q > 1$ (Lovejoy and Schertzer, 2013). If the intermittency is weak, we can reasonably infer H for structure functions with $q > 1$ using the equation $H \approx \zeta(q)/q$ with the expectation that this method may slightly underestimate H. The main text used this method for $q = 2$. In Figs. S3-S6 we reproduce the Figs. 4-8 for first order structure functions, where it is expected that $\zeta = H$ for a multiplicative cascade (Lovejoy and Schertzer, 2013), and for $q = 3$ for comparison with other prior studies. Table S1 lists the calculated exponents derived from structure functions calculated for $q = 1$, $q = 2$, and $q = 3$.

Table S1: Structure function exponents for orders $q = 1, 2, 3$ (Eqn. S2) and estimated values for the Hurst exponent.

Dataset	Direction	Order (q)	Structure Function Exponent $\zeta(q)$	Inferred $H = \zeta(q)/q$
IGRA	Vertical	1	0.62 ± 0.02	0.62 ± 0.02
		2	1.24 ± 0.04	0.62 ± 0.02
		3	1.80 ± 0.06	0.60 ± 0.02
ACTIVATE	Vertical	1	0.70 ± 0.01	0.70 ± 0.01
		2	1.43 ± 0.03	0.71 ± 0.01
		3	2.12 ± 0.04	0.71 ± 0.01
Hurricanes	Vertical	1	0.523 ± 0.007	0.523 ± 0.007
		2	1.03 ± 0.02	0.513 ± 0.008
		3	1.51 ± 0.03	0.504 ± 0.009
IGRA	Horizontal	1	0.49 ± 0.02	0.49 ± 0.02
		2	1.00 ± 0.04	0.50 ± 0.02
		3	1.44 ± 0.04	0.48 ± 0.01

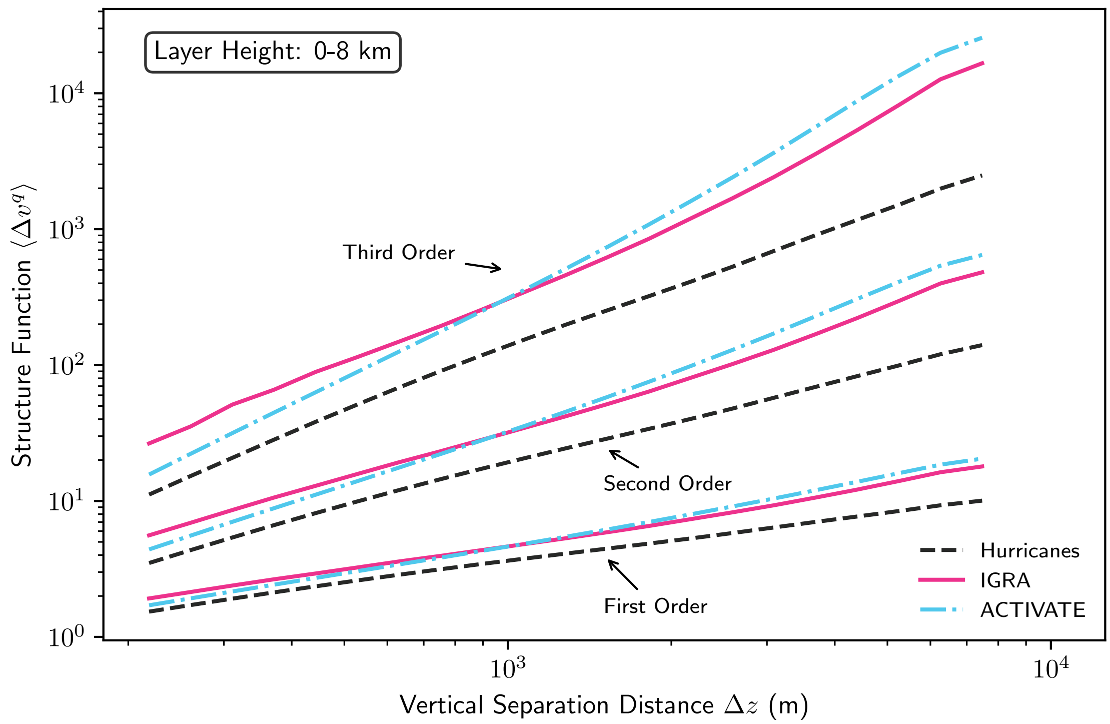

Figure S3: As in Fig. 4, but for first-, second-, and third-order structure functions $\langle \Delta v^2 \rangle$ (lower), $\langle \Delta v^2 \rangle$ (middle) and $\langle \Delta v^3 \rangle$ (upper).

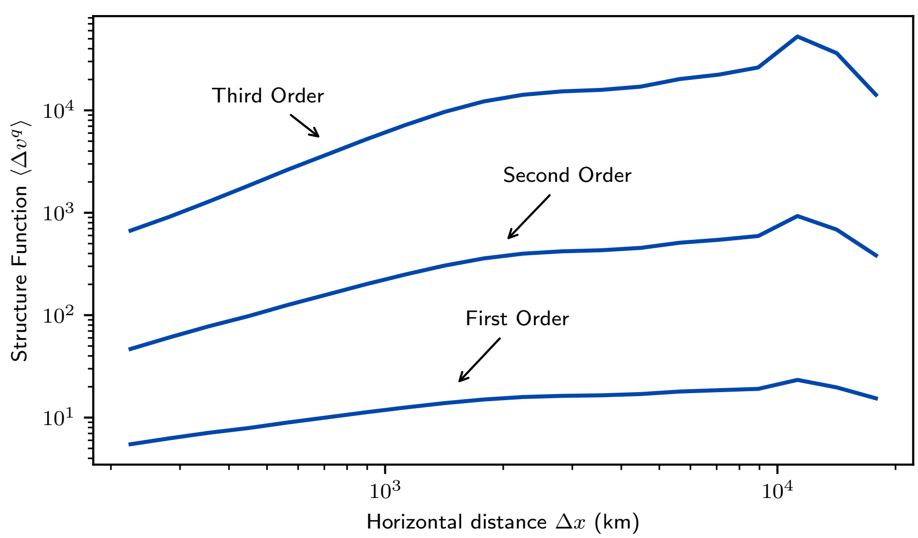

Figure S4: As in Fig. 6, but for first-, second-, and third-order structure functions $\langle \Delta v^2 \rangle$ (lower), $\langle \Delta v^2 \rangle$ (middle) and $\langle \Delta v^3 \rangle$ (upper).

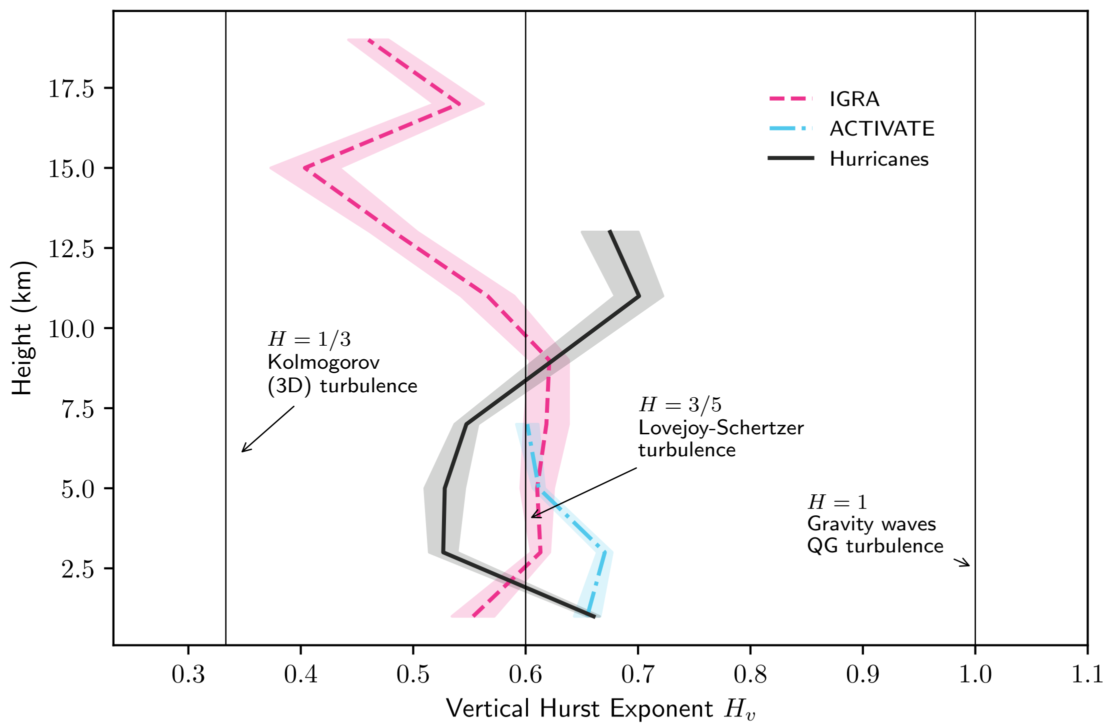

Figure S5: As in Fig. 5, but for first-order structure functions $\langle \Delta v \rangle$.

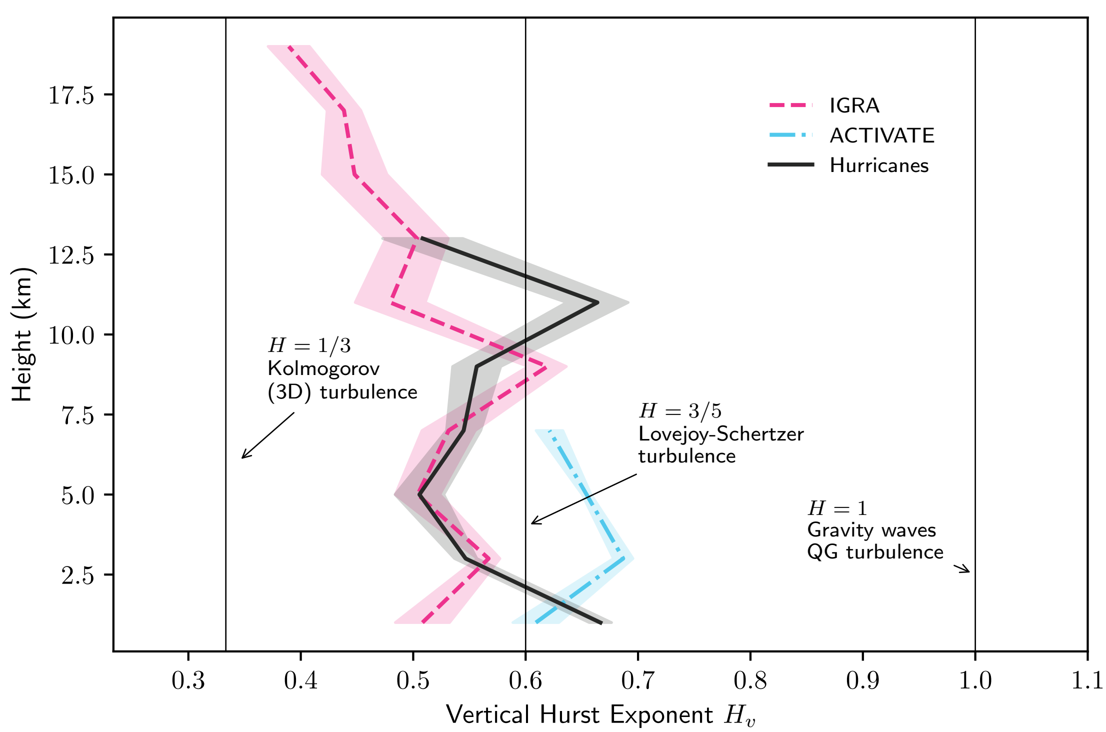

Figure S6: As in Fig. 5, but for third-order structure functions $\langle \Delta v^3 \rangle$.

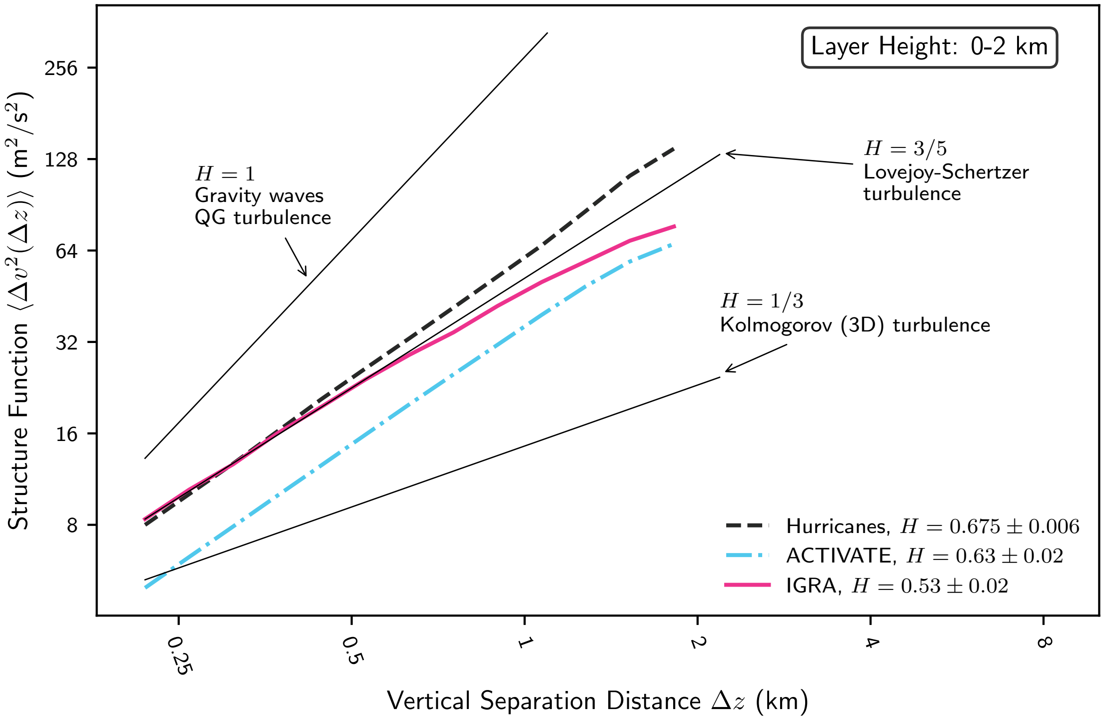

Figure S7: As in Fig. 4, but for altitudes between 0 and 2 km.

S3 Structure functions for individual 2 km-thick layers

Figures S7 to S16 display the structure functions for each altitude layer that were used to calculate H_v as a function of height in Fig. 5.

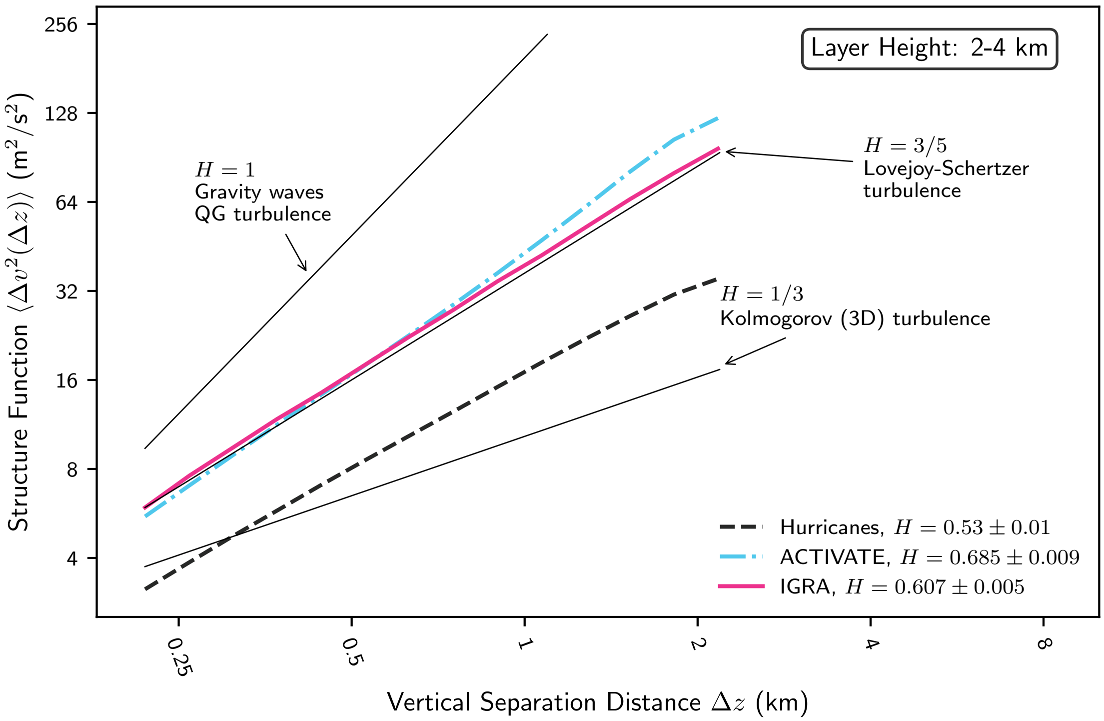

Figure S8: As in Fig. 4, but for altitudes between 2 and 4 km.

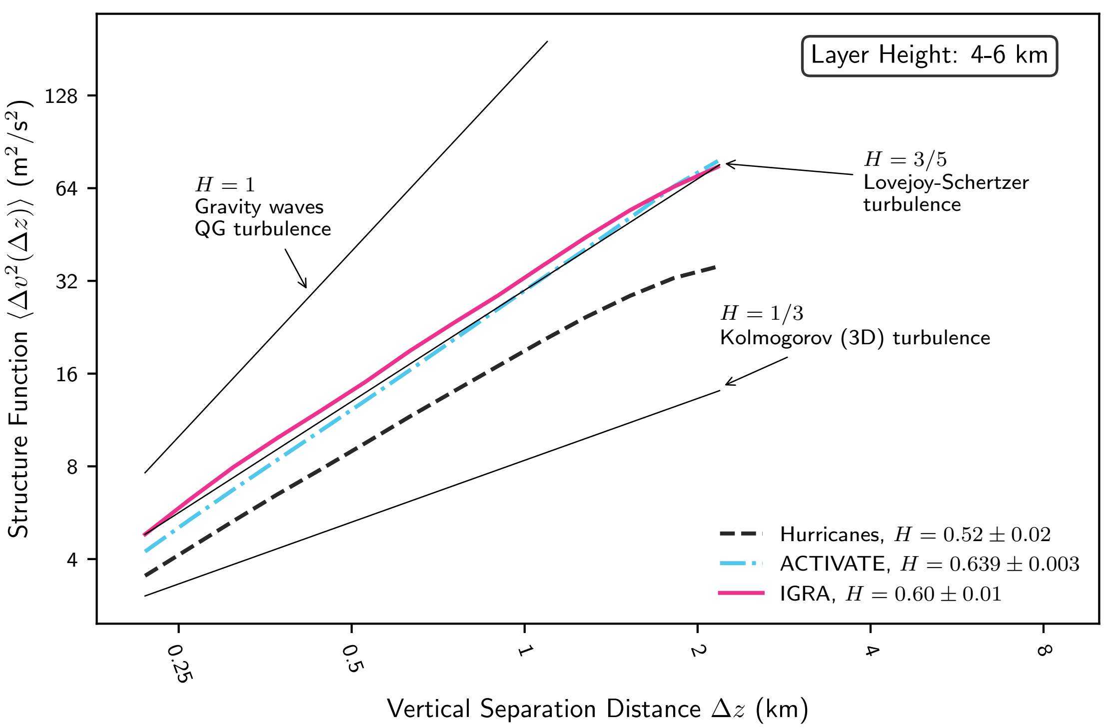

Figure S9: As in Fig. 4, but for altitudes between 4 and 6 km.

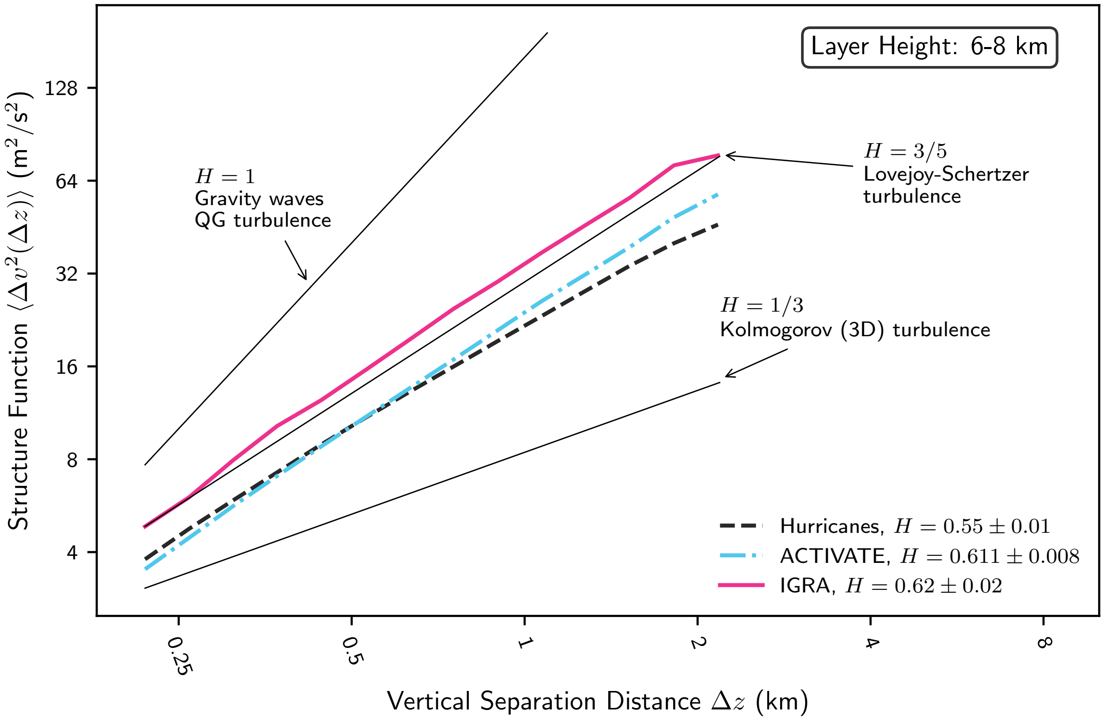

Figure S10: As in Fig. 4, but for altitudes between 6 and 8 km.

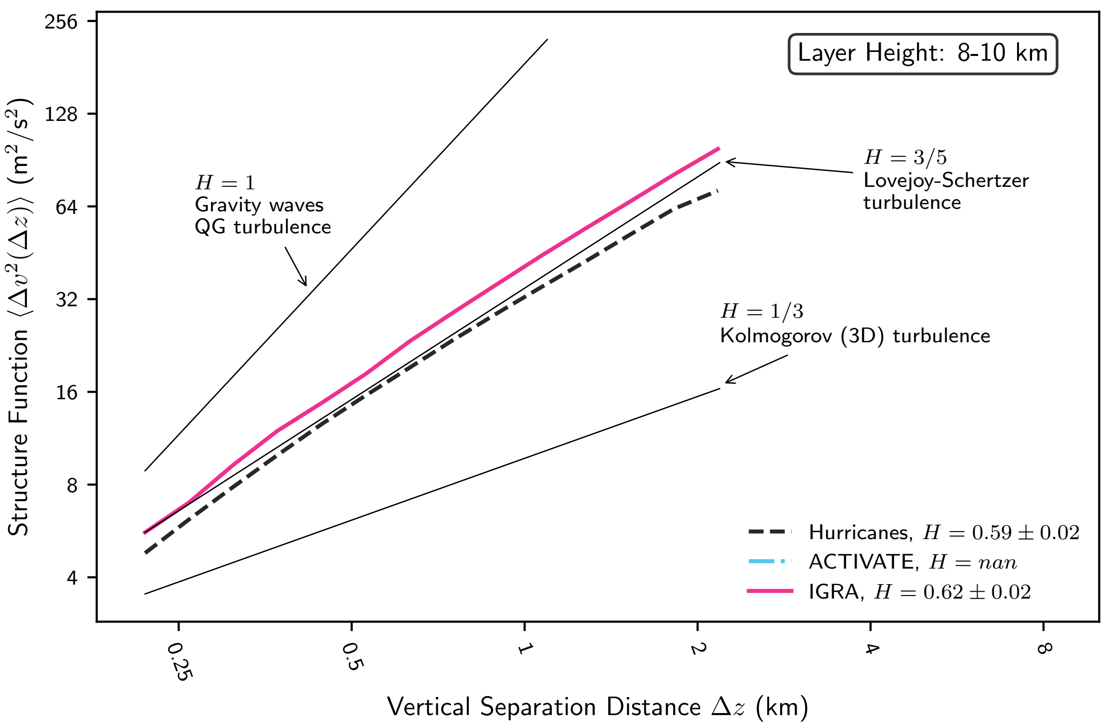

Figure S11: As in Fig. 4, but for altitudes between 8 and 10 km.

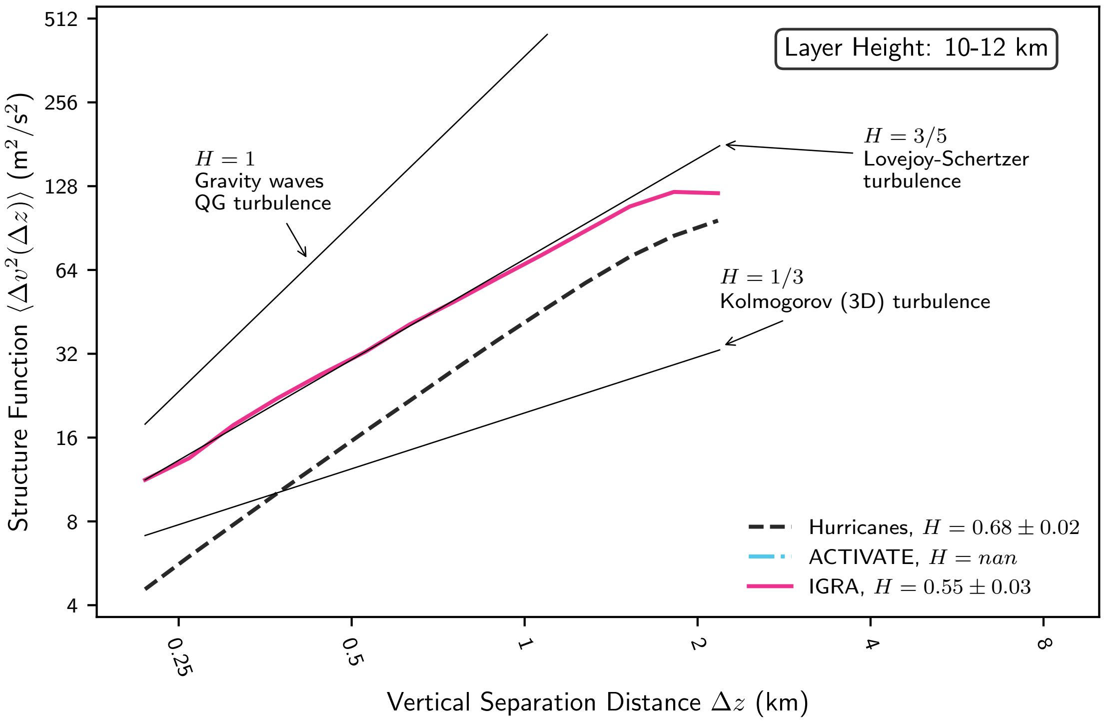

Figure S12: As in Fig. 4, but for altitudes between 10 and 12 km.

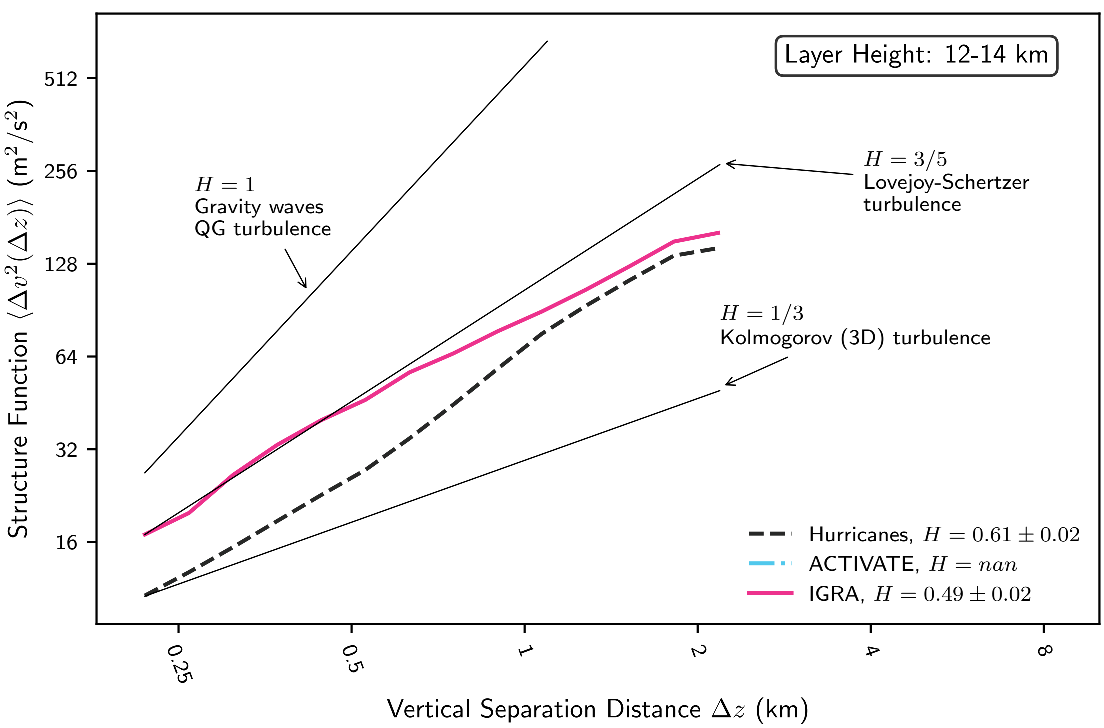

Figure S13: As in Fig. 4, but for altitudes between 12 and 14 km.

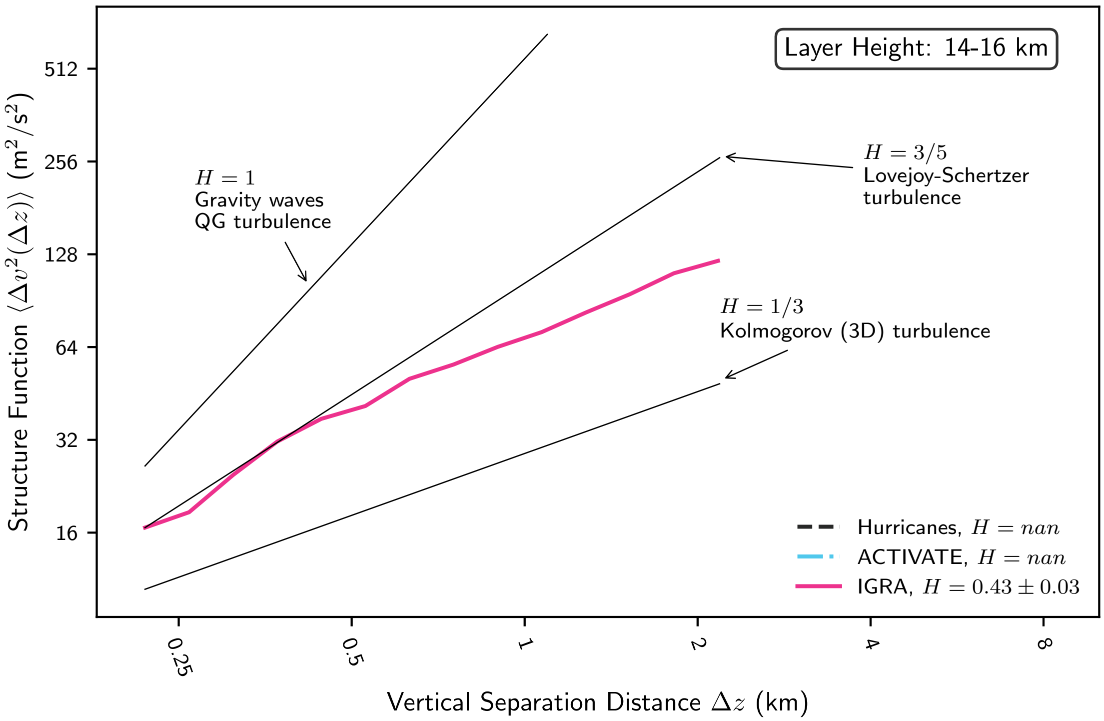

Figure S14: As in Fig. 4, but for altitudes between 14 and 16 km.

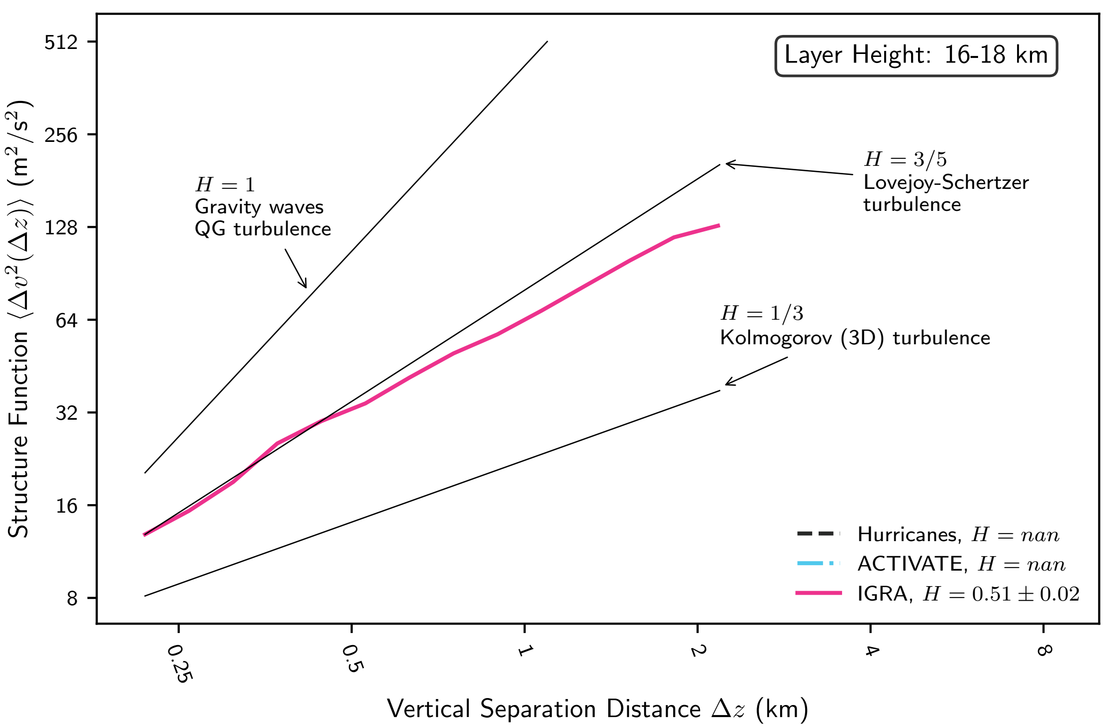

Figure S15: As in Fig. 4, but for altitudes between 16 and 18 km.

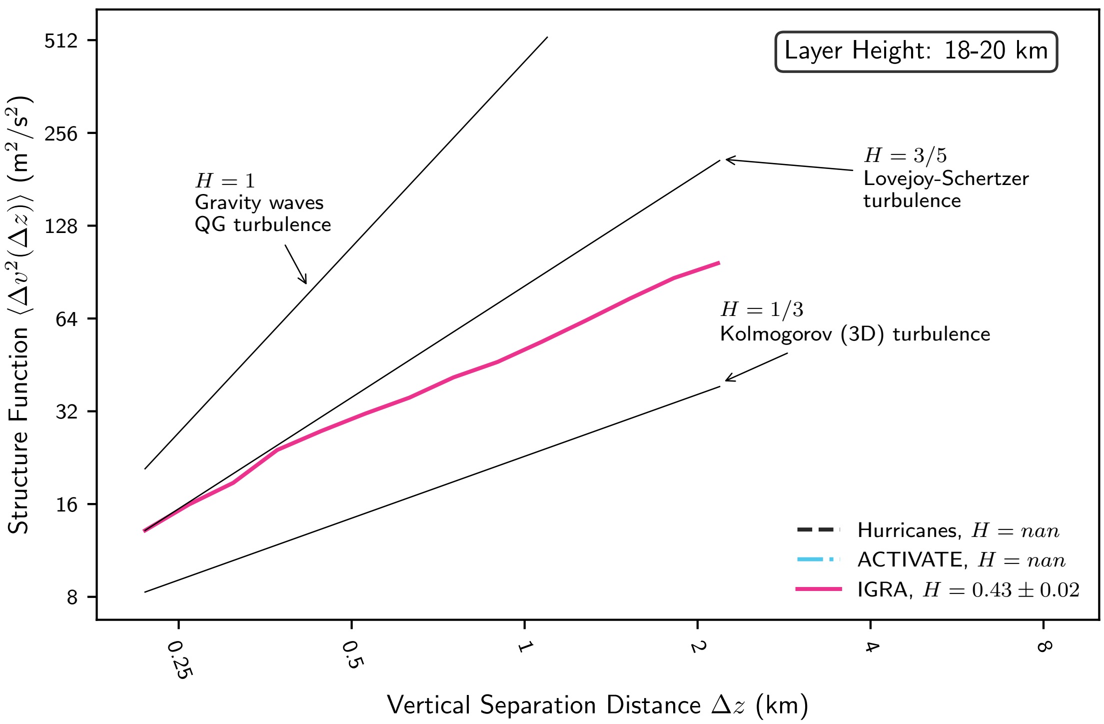

Figure S16: As in Fig. 4, but for altitudes between 18 and 20 km.

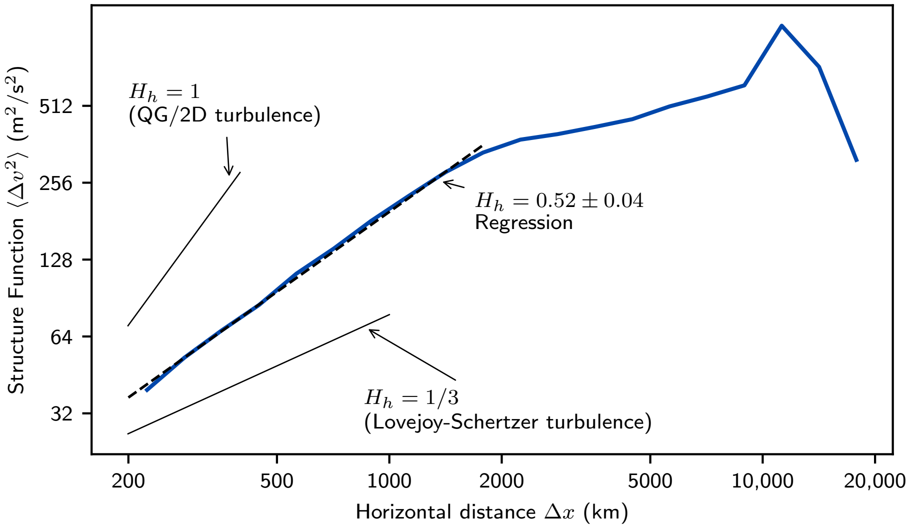

Figure S17: As in Fig. 6, but for observation pairs separated by at most 5 minutes and 5 m in altitude.

S4 Additional horizontal structure functions

In this section we report four additional horizontal structure functions calculated from IGRA data. Figure S17 shows a horizontal structure function as in Fig. 6 but for observation pairs separated by at most 5 minutes and 5 m in altitude as described in Section 3.1.

Figure S18 shows a structure function calculated for observation pairs between -20° and 20° in latitude, while Fig. S19 shows a structure function calculated for observation pairs between 45° and 90° in latitude.

Figures S20 and S21 show horizontal structure functions for temperature variance T^2 and pressure variance p^2, respectively, rather than kinetic energy.

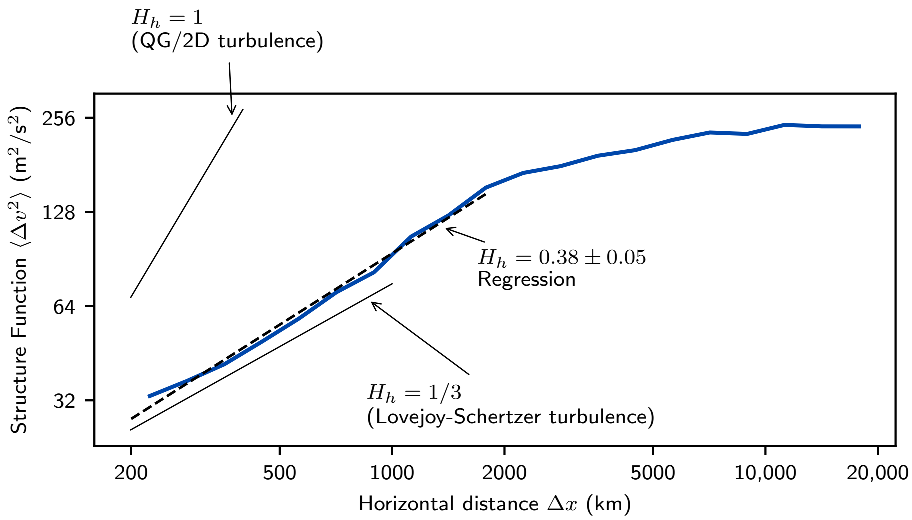

Figure S18: As in Fig. 6, but for observation pairs between -20° and 20° in latitude.

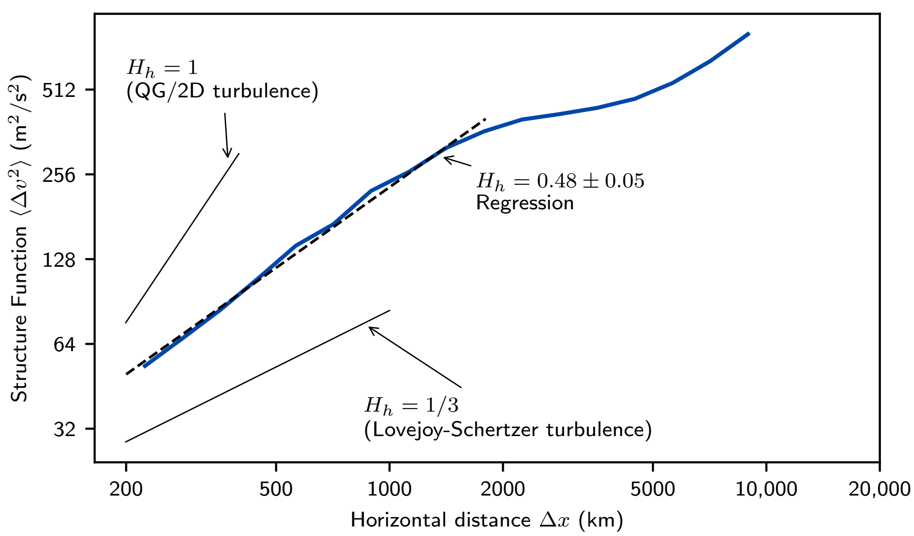

Figure S19: As in Fig. 6, but for observation pairs between 45° and 90° in latitude.

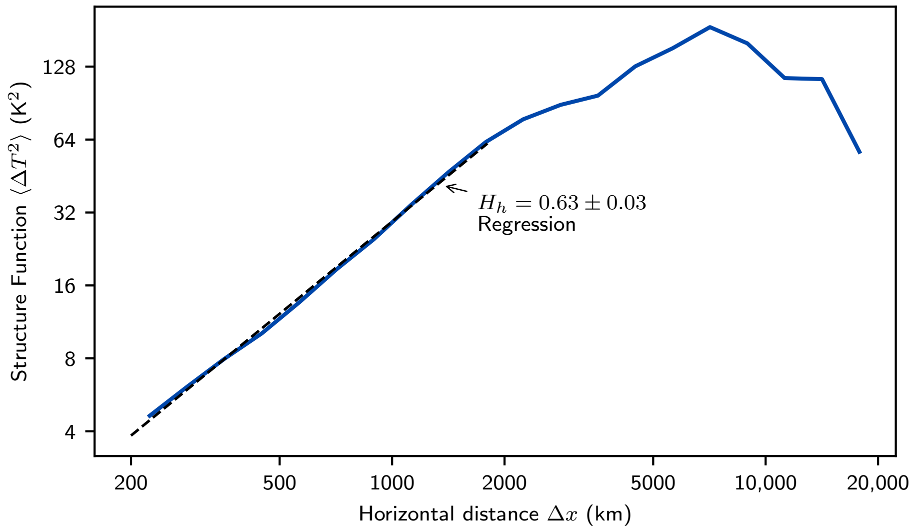

Figure S20: As in Fig. 6, but for temperature T rather than kinetic energy, where $\Delta T^2 \sim \Delta x^{2H_h}$.

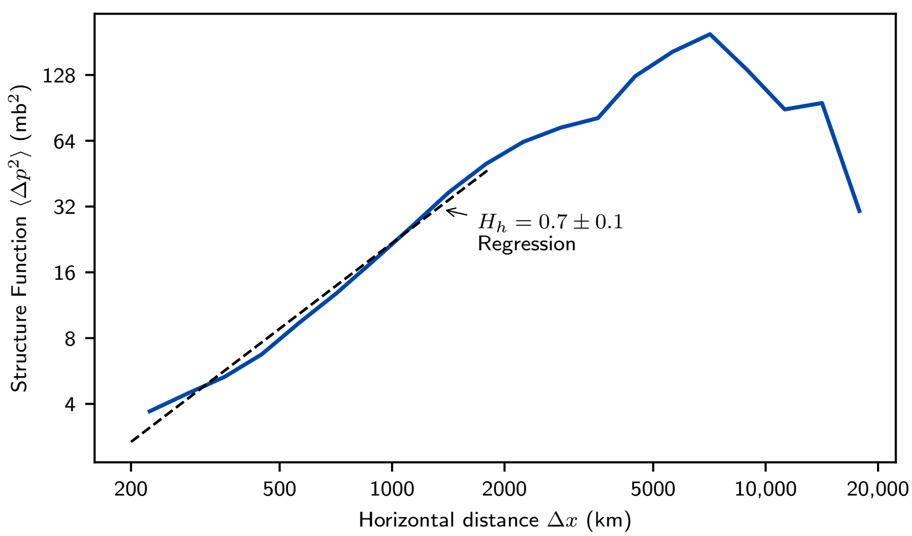

Figure S21: As in Fig. 6, but for pressure p rather than kinetic energy, where $\Delta p^2 \sim \Delta x^{2H_h}$.

References

Lovejoy, S. and Schertzer, D.: The weather and climate: emergent laws and multifractal cascades, Cambridge University Press, 2013.